mathematics

MDPI

Article

On Consequences of Carreau Nanofluid Model with Dufour–Soret Effects and Activation Energy Subject to New Mass Flux Condition: A Numerical Study

Usman Ali * and Mawia Osman

School of Mathematical Sciences, Zhejiang Normal University, Jinhua 321004, China
* Correspondence: usmanali@zjnu.edu.cn

Abstract: Activation energy can be elaborated as the minimal energy required to start a certain chemical reaction. The concept of this energy was first presented by Arrhenius in the year 1889 and was later used in the oil reservoir industry, emulsion of water, geothermal as well as chemical engineering and food processing. This study relates to the impacts of mass transfer caused by temperature differences (Soret) and heat transport due to concentration gradient (Dufour) in a Carreau model with nanofluids (NFs), mixed convection and a magnetic field past a stretched sheet. Moreover, thermal radiation and activation energy with new mass flux constraints are presumed. All chemical science specifications of nanofluid are measured as constant. As a result of the motion of nanofluid particles, the fluid temperature and concentration are inspected, with some physical description. A system of coupled partial differential frameworks is used mathematically to formulate the physical model. A numerical scheme named the Runge–Kutta (R-K) approach along with the shooting technique are used to solve the obtained equations to a high degree of accuracy. The MATLAB R2022b software is used for the graphical presentation of the solution. The temperature of the nanofluid encompasses a quicker rate within the efficiency of a Dufour number. An intensifying thermal trend is observed for thermophoresis and the Brownian motion parameter. The Soret effect causes a decline in the fluid concentration, and the opposite trend is observed for rising activation energy. In addition, the local Nusselt number increases with the Prandtl number. Further, the comparative outcomes for drag force are established, with satisfying agreement with the existing literature. The results acquired here are anticipated to be applied to improving heat exchanger thermal efficiency to maintain thermal balancing control in compact heat density equipment and devices.

Keywords: Carreau model; nanofluid; Soret–Dufour effects; activation energy; new mass flux conditions

MSC: 76-10

check for updates

Citation: Ali, U.; Osman, M. On Consequences of Carreau Nanofluid Model with Dufour–Soret Effects and Activation Energy Subject to New Mass Flux Condition: A Numerical Study. *Mathematics* **2023**, *11*, 2564. https://doi.org/10.3390/math11112564

Academic Editor: Vasily Novozhilov

Received: 25 April 2023
Revised: 19 May 2023
Accepted: 30 May 2023
Published: 3 June 2023

1. Introduction

It is evident that non-Newtonian fluids fail to follow Newton's law of viscosity. For proper engineering of non-Newtonian fluids, viscosity is obviously dependent on shear stress and time. Due to non-Newtonian fluid variations, several basic equations have been proposed. Recently, a growing interest in the biotechnology era has been explored due to industrial and technological applications. Nanomaterials are the most complex mixtures and have extraordinary special properties. Such microscopic particles are highly promoted, more healthy and environmentally friendly. Due to their extremely high degree of confrontation and diverse properties, nanomaterials have become the center of integration in chemical, mechanical and biotechnology industries, such as in nuclear reactors, fission reactions, chemical oxidation, camera technology, diagnosis and treatment I of cancer tissue, catalysis, brain tumors, engineering and much more. The theoretical properties of nanomaterials to improve thermal extrusion mechanisms focus on the importance of low-energy reservoirs. The "nanofluid" base extension was introduced by Choi [1], and the experimental data confirmed that thermal transmission is effectively raised by employing small metal nanomaterials in the base fluid. Buongiorno [2] found that the thermophoretic diffusion and Brownian motion of nanofluids are important processes for increasing the transient heat transfer coefficient. Nanofluid flow research has made outstanding contributions to science in the current period due to its scope of application for power generation, as cooling devices in vehicles, expertise in refrigerant processing and various biochemical applications used in cancer assessment in many fields. The thermal conductivity of this critical fluid plays a decisive role in the heat transfer coefficient between the heat carrier and the metal sheet. A detailed description of the theoretical study of a nanofluid's thermal conductivity with suspension of copper nanophase powder is given in [3]. The study of nanofluids with a transverse magnetic field, buoyancy effects and thermal radiation invoked by a stretching sheet is discussed by Rashidi et al. [4]. Malvandi et al. [5] investigated the two-dimensional stagnation point flow of a nanofluid over a stretching sheet. A comprehensive overview summarizing the usage of thermal conduction in nanofluids with some experimental studies is provided by Das [6]. Atashafrooz et al. [7] studied the hybrid nanofluid model in a convective radiative flow field through an open trapezoidal enclosure to determine heat transfer analysis via various radiative parameters. The factors affecting thermal conductivity are discussed in this article, including nanoparticle types, solid volume fraction, different base fluids, temperature and different mechanisms for increasing thermal conductivity in nano liquid development. Further specifications of nanofluid can be seen in Refs. [8,9].

Of the numerous models introduced in the literature for non-Newtonian fluids, there is one more useful proposed by Carreau [10,11] (Carreau fluid or the generalized-Newtonian fluid). This fluid model is an amalgamation of Newtonian fluid and the power law model. This reveals shear-thinning properties at low shear rates and shear thickening property at higher shear rates. Carreau fluid is of great concern for many engineers because of its importance in the suspension of polymers, aqueous and melting, etc. Several researchers have discussed the importance of such a model when studying the performance of Carreau fluids with various geometries. A few of the relevant Carreau fluid flow analyses are provided. The features of nanoparticles in the presence of a generalized Carreau fluid model with suction/injection parameters and thermal radiation through a non-linear stretching surface were observed by Eid et al. [12]. A study of Carreau fluid through an inclined stretching surface was conducted by Khan et al. [13]. The specifications of Carreau fluid at a stagnation point through a shrinking plate were debated by Akbar et al. in [14]. The numerical results for the transport of heat and mass in a Carreau fluid produced by a magnetic field with cross-diffusion were studied in [15]. Entropy generation in a Carreau fluid with thermal radiation through a stretching sheet was studied by Raza et al. [16]. The temperature-dependent thermophysical properties, such as thermal diffusivity and thermal conductivity, in Carreau liquid with activation energy and heat generation were studied by Salahuddin et al. [17].

It is evident that the temperature and concentration gradients represent mass and energy fluxes, respectively. The concentration gradient causes the Dufour effect (thermos diffusion), while the Soret effect (thermos diffusion) is caused by a temperature gradient. Such an effect plays an important role in the difference in flux density. Huang [18] investigated the effects of Soret–Dufour in a non-Newtonian fluid in the presence of MHD suction/injection and thermal radiation phenomena. The Soret–Dufour effects combined with mixed convection and thermal radiation in a viscoelastic fluid was debated by Mahabaleshwar et al. [19]. Further relevant literature is found in [20–23].

A thorough analysis of the existing literature suggests that stretched flow caused by an extended surface rarely confers a nanofluid with Dufour–Soret effects and new mass flux condition (Wang [24]). The 2-dimensional Carreau stretched flow was studied by Khan et al. [13]. Here, the restriction relates to the base fluid's lower capacity for heat conduction, which leads to ineffective thermal transmission. The main driving force behind this effort is the addition of nanoparticles to MHD to improve thermal conductivity and provide effective heat transport. The three-dimensional fluid flow is meant to be constant. The flow is restricted in the portion $z > 0$ and occurs over a region that fits the plane $z = 0$. To keep the sheet extended and the origin as constant, two balanced forces were applied in opposition along the $x-$ axis. The z-axis is perpendicular to the sheet. However, the Dufour–Soret effect, mixed convection, and activation energy subject to new mass flux condition are chosen as novel components of this work. The model was also created to assess how Brownian motion and thermophoresis behave. By eliminating some specific terms, this problem can be reduced to Ref. [13], which shows the novelty of the proposed problem. A numerical assessment named shooting scheme with an R-K approach (Ali et al. [25]) is implied on the obtained ODEs to obtain the numerical solutions. The curves are designed to show the behavior of temperature and concentration profiles against thermophoresis, thermal radiation, Dufour–Soret effects, Brownian motion and activation energy parameters. In addition, the numerical values for the drag force and rate of thermal and mass flux are shown in Tables 1–3 and compared with the existing literature to show the accuracy and efficiency of the current method.

Table 1. Table for $-f''(0)$ corresponding to a variety of values of α when $N^* = M = We_1 = We_2 = 0$, $n = 1$.

α	$-f''(\mathbf{0})$ [24]	$-f''(\mathbf{0})$ **Current Results**
0	-1	-1
0.25	-1.048813	-1.048813
0.50	-1.093097	-1.093097
0.75	-1.134485	-1.134485
1	-1.173720	-1.173720

Table 2. Table for $-g''(0)$ corresponding to a variety of values of α when $N^* = M = We_1 = We_2 = 0$, $n = 1$.

α	$-g''(\mathbf{0})$ [24]	$-g''(\mathbf{0})$ **Current Results**
0	0	0
0.25	-0.194564	-0.194564
0.50	-0.465205	-0.465205
0.75	-0.794622	-0.794622
1	-1.173720	-1.173720

Table 3. Table for Nusselt number corresponding to a variety of values of Pr when $N^* = We_1 = We_2 = \alpha = n = \lambda^* = N_b = N_t = Sr = Dr = \Lambda^* = Le = 0$.

Pr	Nu_x **Ref. [13]**	$N\widetilde{u}_x$ **Current Results**
0.7	0.454501	0.454525
2.0	0.911411	0.912131
7.0	1.895400	1.876201

2. Problem Conceptualization

Consider the three-dimensional incompressible Carreau fluid model across the stretched sheet. The coordinate axis is depicted as the x—axis along the stretching sheet and the z—axis perpendicular to the sheet. The fluid flows at $z > 0$. The sheet velocity is considered as $u = U_w(x) = ax$ with $a > 0$ as the stretching rate and $v = V_w(y) = by$ where $b > 0$. The magnetic field $B_\circ$ is towards the z-axis (see Figure 1), and for a lesser Reynold's number, the induced magnetic field is considered as negligible. The energy equation is constructed in addition to the mechanism of nonlinear thermal radiation. Furthermore, thermal transport using Brownian and thermophoresis nanoparticles is reported. The concentration field is arranged under the effects of a binary chemical reaction with Arrhenius activation energy. This idea is formulated and leads to the following equations. The Carreau fluid model by Khan et al. [12] is precisely defined as below:

$$\begin{aligned} &\hat{\tau} = -Ip + \mu(\dot{\gamma})A_1\,, \\ &\mu = \mu_\infty + (\mu_0 - \mu_\infty)[(\Gamma\dot{\gamma})^2 + 1]^{\frac{n-1}{2}}\,, \end{aligned} \tag{1}$$

where the Cauchy stress tensor is $\hat{\tau}$, p is the pressure, I is the identity tensor, A_1 is the first Rivlin Erickson tensor, $\dot{\gamma} = \sqrt{\frac{1}{2}\Pi}$ with Π is a second invariant strain tensor and defined as $\Pi = \mathrm{tr}(A_1^2)$ (tr is trace), the power law index is n, the material time constant is Γ and the zero and infinite shear rate viscosities are $\mu_\circ$ and μ_∞, which is less than the ones here. These assumptions are made, and the resulting flow model arises as Refs. [12,21],

$$\frac{\partial w}{\partial z} + \frac{\partial v}{\partial y} + \frac{\partial u}{\partial x} = 0, \tag{2}$$

$$\begin{aligned} &\tfrac{\partial u}{\partial x}u + \tfrac{\partial u}{\partial y}v + \tfrac{\partial u}{\partial z}w = v\tfrac{\partial^2 u}{\partial z^2}[1 + \Gamma^2(\tfrac{\partial u}{\partial y})^2]^{\frac{n-1}{2}} \\ &+\Gamma^2(n-1)v(\tfrac{\partial^2 u}{\partial z^2})(\tfrac{\partial u}{\partial z})^2\left[\Gamma^2(\tfrac{\partial u}{\partial y})^2 + 1\right]^{\frac{n-3}{2}} - u\tfrac{\sigma B_\circ^2}{\rho_f} \\ &+g[\beta_T(T - T_\infty) + \beta_c(C - C_\infty)], \end{aligned} \tag{3}$$

$$\begin{aligned} &\tfrac{\partial v}{\partial x}u + \tfrac{\partial v}{\partial y}v + \tfrac{\partial v}{\partial z}w = v\left[\Gamma^2(\tfrac{\partial v}{\partial z})^2 + 1\right]^{(\frac{n-1}{2})}\tfrac{\partial^2 v}{\partial z^2} \\ &+\Gamma^2(n-1)v(\tfrac{\partial^2 v}{\partial z^2})(\tfrac{\partial v}{\partial z})^2\left[\Gamma^2(\tfrac{\partial u}{\partial y})^2 + 1\right]^{\frac{n-3}{2}} - \tfrac{\sigma B_\circ^2}{\rho_f}v, \end{aligned} \tag{4}$$

$$\frac{\partial T}{\partial x}u + \frac{\partial T}{\partial y}v + \frac{\partial T}{\partial z}w = \alpha_1(\frac{\partial^2 T}{\partial z^2}) + \tau\left[D_B\frac{\partial T}{\partial z}\frac{\partial C}{\partial z} + \frac{D_T}{T_\infty}(\frac{\partial T}{\partial z})^2\right] - \frac{1}{(\rho c)_f}\frac{\partial q_r}{\partial z} + \frac{D_m k_T}{c_s c_p}\frac{\partial^2 C}{\partial z^2}, \tag{5}$$

$$\begin{aligned} &\tfrac{\partial C}{\partial x}u + \tfrac{\partial C}{\partial y}v + \tfrac{\partial C}{\partial z}w = \tfrac{D_T}{T_\infty}(\tfrac{\partial T}{\partial z})^2 + \tfrac{\partial^2 C}{\partial z^2}D_B \\ &-[C - C_\infty]k_c^2\left(\tfrac{T}{T_\infty}\right)^m \exp\left(\tfrac{-E^*}{\kappa T}\right) + \tfrac{D_m k_T}{T_m}\tfrac{\partial^2 T}{\partial z^2}, \end{aligned} \tag{6}$$

$$\begin{aligned} &u = ax = U_w(x),\ v = by = V_w(y),\ T_w = T,\ D_B\left(\tfrac{\partial C}{\partial z}\right) = -\tfrac{D_T}{T_\infty}\left(\tfrac{\partial T}{\partial z}\right) \text{ at } z = 0, \\ &u \to 0, v \to 0,\ T \to T_\infty,\ C \to C_\infty \text{ as } z \to \infty, \end{aligned} \tag{7}$$

where the velocity components in the x, y and z-directions are suggested as (u, v, w) and the kinematic viscosity and electrical conductivity are v and σ, respectively. The thermal and concentration expansions are β_T and β_c. The ratio of heat capacity of nanoparticles and base liquids is τ. Moreover, $\alpha_1, \rho_f, c_f, D_T, D_B$ are the thermal diffusivity, density of fluid, specific heat, thermal and Brownian coefficients of diffusion. Further, E^* signifies activation energy, whereas m $(-1 < m < 1)$ is the fitted rate constant, k_c is the chemical reaction rate and $\kappa = 8.61 \times 10^5 \mathrm{eV/K}$ is the Boltzmann constant. Thus, the whole term that is $k_c(\frac{T}{T_\infty})^m exp\left(-\frac{E^*}{\kappa T}\right)$, named the Arrhenius equation in modified form. The thermal radiation via the Rosseland approximation and, hence, radiative heat flux q_r is defined as $q_r = \frac{-16\sigma^* T_\infty^3}{k^*}\frac{\partial T}{\partial z}$ where σ^* is indicated as the Stefan–Boltzmann constant and k^* is the coefficient of the mean absorption. The suitable transformations are as follows:

$$\begin{aligned} &u = axf'(\eta),\ v = ayg'(\eta), w = 0,\ \phi(\eta) = \tfrac{C-C_\infty}{C_\infty},\\ &\theta(\eta) = \tfrac{T-T_\infty}{T_f-T_\infty},\ \eta = z\sqrt{\tfrac{a}{v}}, \end{aligned} \tag{8}$$

the stream function ψ satisfies the continuity equation where $u = \frac{\partial\psi}{\partial y}, v = -\frac{\partial\psi}{\partial x}$. The transformed equations are as follows:

$$\left[1 + We_1^2 (f'')^2\right]\left[1 + nWe_1^2 (f'')^2\right]^{\frac{n-3}{2}} f''' + (f+g)f'' - (f')^2 + \lambda^*\theta + \lambda^* N^*\phi - M^2 f' = 0, \tag{9}$$

$$g'''\left[n(g'')^2 We_2^2 + 1\right]^{\frac{n-3}{2}}\left[1 + We_2^2 (g'')^2\right] - (g')^2 + g''[g+f] - M^2 g' = 0, \tag{10}$$

$$\left(1 + \frac{4R}{3}\right)\theta'' + (g+f)\Pr\theta' + \Pr\left(N_t \theta'^2 + N_b\theta'\phi'\right) + Dr\phi'' = 0, \tag{11}$$

$$\phi'' + \Pr Le(f+g)\phi' + \frac{N_t}{N_b}\theta'' + LeSr\theta'' - Le\Pr\Lambda(1+\Lambda^*\theta)^m \phi\exp\left[\frac{-E}{1+\Lambda^*\theta}\right] = 0 \tag{12}$$

The following involved non-dimensional parameters are defined and described as

$$\begin{aligned} &We_1 = \sqrt{\tfrac{\Gamma^2 a U_w^2}{v}}, We_2 = \sqrt{\tfrac{\Gamma^2 a V_w^2}{v}}, M^2 = \tfrac{\sigma B_\circ^2}{\rho\alpha}, \lambda^* = \tfrac{g\beta_T(T_f - T_\infty)}{aU_w}, \alpha = \tfrac{b}{a},\\ &N^* = \tfrac{g\beta_c(C_f - C_\infty)}{\beta_T(T_f - T_\infty)}, R = \tfrac{4\sigma^* T_\infty^3}{kk^*}, N_b = \tfrac{\tau D_B}{v}(C_f - C_\infty), N_t = \tfrac{D_T}{vT_\infty}(T_f - T_\infty), \Pr = \tfrac{v}{\alpha_1},\\ &\Lambda = \tfrac{k_r^2}{a}, \Lambda^* = \tfrac{T_f - T_\infty}{T_\infty}, E = \tfrac{E^*}{\kappa T_\infty}, Dr = \tfrac{D_B K_T(C_f - C_\infty)}{vc_p c_s(T_f - T_\infty)}, Sr = \tfrac{D_B K_T(T_f - T_\infty)}{vT_m(C_f - C_\infty)}, Le = \tfrac{\alpha_1}{D_B} \end{aligned} \tag{13}$$

where We_1 and We_2 are local Weissenberg numbers, M^2 is the magnetic field, λ^* is a parameter of mixed convection, α is the velocity ratio parameter, N^* is the buoyancy ratio parameter, R is the thermal radiation parameter, N_b, N_t are the Brownian motion and thermophoresis parameters, Pr is the Prandtl number, Λ is the reaction rate parameter, Δ^* is the temperature difference parameter, E is the activation energy parameter, Dr is Dufour, Sr is the Soret number and Le is the Lewis number. The relevant constraints are as follows:

$$\begin{aligned} &(f(0) = 0);\ \ (0) = 0,\ f'(0) = 1,\ g'(0) = \alpha,\ (\theta(0) = 1),\\ &(-N_t\theta'(0) = N_b\phi'(0))\ \text{when}\ \eta = 0,\\ &(f' \to\ 0;\ \ g' \to\ 0);\ \ (\theta \to\ 0;\ \ \phi \to\ 0)\ \text{as}\ \eta \to \infty, \end{aligned} \tag{14}$$

The parameters for engineering use are termed as

$$C_{fx} = \frac{2\tau_{xz}}{\frac{1}{2}\rho_f U_w^2(x)},\ C_{fy} = \frac{\tau_{yz}}{\frac{1}{2}\rho_f U_w^2(x)}, \tag{15}$$

$$Nu_x = \left(\frac{-x}{(T_f - T_\infty)} - \frac{x\,q_r}{k\,(T_\infty - T_f)}\right)\left(\frac{\partial T}{\partial z}\right)_{z=0}, Sh_x = \frac{-x}{(C_f - C_\infty)}\left(\frac{\partial C}{\partial z}\right)_{z=0} \tag{16}$$

the dimensionless form of the aforementioned quantities is defined as

$$\begin{aligned} &\tfrac{1}{2}\mathrm{Re}_x^{1/2} C_{fx} = f''(0)\left[1 + We_1^2 f''^2(0)\right]^{\frac{n-1}{2}},\ \ \tfrac{1}{2}\left(\tfrac{U_w}{V_w}\right)\mathrm{Re}_x^{1/2} C_{fy} = g''(0)\left[1 + We_2^2 g''^2(0)\right]^{\frac{n-1}{2}}\\ &\mathrm{Re}^{-1/2} Nu_x = -\left(1 + \tfrac{4}{3}R\right)\theta'(0),\ \mathrm{Re}^{-1/2} Sh_x = -\phi'(0), \end{aligned} \tag{17}$$

where $\mathrm{Re}_x = \frac{ax^2}{v}$ is the local Reynolds number.

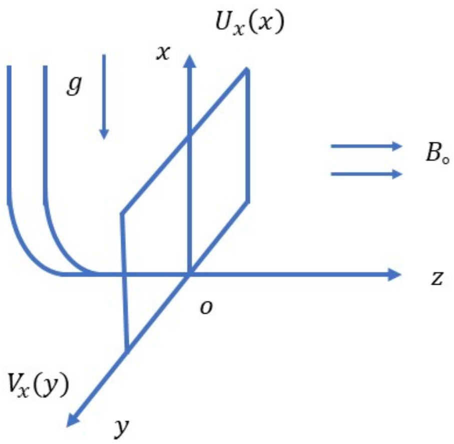

Figure 1. Physical illustration of the problem.

3. Numerical Algorithm

The governing equations Equations (9)–(12) are highly nonlinear in a coupled form. So, we convert them into a first-order system, and then we apply shooting technique with fourth–fifth-order scheme to solve the system. We may write

$$f''' = \frac{(f')^2 - f''(f+g) + M^2 f' - \lambda^* \theta^2 - \lambda^* N^* \phi^2}{\left[1 + nWe_1^2 (f'')^2\right]^{\frac{n-3}{2}} \left[1 + We_1^2 (f'')^2\right]}, \tag{18}$$

$$g''' = \frac{(g')^2 - g''(f+g) + M^2 g'}{\left[1 + nWe_1^2 (g'')^2\right]^{\frac{n-3}{2}} \left[1 + We_1^2 (g'')^2\right]}, \tag{19}$$

$$\theta'' = -\left(\frac{3}{3+4R}\right)\left[-\Pr\theta'(f+g) - \Pr(N_t \theta'^2 + N_b \theta' \phi') - Dr\phi''\right], \tag{20}$$

$$\phi'' = (f+g) Le \Pr \phi' - \frac{N_t}{N_b}\theta'' + \Pr Le\, \Lambda (1 + \Lambda^* \theta)^m \phi \exp\left[\frac{-E}{1 + \Lambda^* \theta}\right], \tag{21}$$

the aforementioned set of higher-order DEs is reduced to first-order ODEs, and we approach new substitutions as follows:

$$\begin{gathered} f = y_1;\ (y_2 = f' = y_1');\ y_3 = y_2' = f'',\ y_4 = g,\ y_5 = g',\ y_6 = g'', \\ (y_6' = g''');\ \theta(\eta) = y_7,\ y_8 = y_7' = \theta',\ (\phi = y_9);\ y_{10} = y_9' = \phi', y_{10}' = \phi'', \end{gathered} \tag{22}$$

by substituting these expressions, we obtain

$$\begin{pmatrix} y_1' = y_2 \\ y_2' = y_3 \\ y_3' = \frac{y_2^2 - y_3(y_1+y_4) + M^2 y_5 - \lambda^* y_7^2 - \lambda^* N^* y_9^2}{[1 + nWe_1^2 y_3^2][1 + We_1^2 y_3^2]^{\frac{n-3}{2}}} \\ y_4' = y_5 \\ y_6' = \frac{y_5^2 - y_6(y_1+y_4) + M^2 y_5}{[1 + nWe_1^2 y_6^2][1 + We_1^2 y_6^2]^{\frac{n-3}{2}}} \\ y_7' = y_8 \\ y_8' = \frac{1}{\left(1 + \frac{4R}{3}\right)}\left(-\Pr(y_1+y_4)y_8 - \Pr(N_b y_8 y_{10} + N_t y_8^2) - Dr\, y'_{10}\right) \\ y_9' = y_{10} \\ y_{10}' = \left(-\Pr Le(y_1+y_4)y_{10} - (\frac{N_t}{N_b})y'_8 - Dr\, y'_{10}\right) \end{pmatrix}, \tag{23}$$

the transformed boundary conditions are

$$\begin{array}{l} y_1(0) = 0, \\ y_2(0) = 1, \;\; y_2(\infty) \to 0, \\ y_3(0) = u_1 \\ y_4(0) = 0, \\ y_5(0) = \alpha, \;\; y_5(\infty) \to 0, \\ y_6(0) = u_2, \\ y_7(0) = 1, \;\; y_7(\infty) \to 0, \\ y_8(0) = u_3, \\ y_9(0) \to u_4, \;\; y_9(\infty) \to 0, \\ y_{10}(0) = -\frac{N_t}{N_b} y_8(0), \end{array} \tag{24}$$

Working Rule

The above-described boundary value dilemma is converted into an initial value problem (IVP) by exchanging the boundary conditions $(y_2(\infty), y_5(\infty), y_7(\infty), y_9(\infty))$, with missing initial conditions $(y_3(0) = u_1, y_6(0) = u_2, \; y_8(0) = u_3, y_9(0) = u_4)$, as the R-K-F (Runge–Kutta–Fehlberg) method only solves IVPs. The IVP is then solved using the R-K-F method with appropriate initial approximations for $(y_3(0), \;\; y_6(0), \;\; y_8(0), \;\; y_9(0))$. If boundary residuals $|y_i(\infty) - \widetilde{y}_i(\infty)|$ for $(i = 2, 5, 7, 9)$, where $\widetilde{y}_i(\infty)$ are computed values, are smaller than tolerance errors, or 10^{-6}, then the computed solution converges. If the calculated results did not satisfy this requirement, the Newton's method is used to update the initial estimates, and the procedure is repeated until the answer satisfies the anticipated convergence principle.

4. Graphical Results and Discussion

When the heat and mass transfer transpire instantly in a fluctuating fluid, such as in geophysical and chemical systems, a cross-diffusion effect happens, named the Soret and Dufour effect. Specifically, the Soret impact is mass transfer due to differences in temperature, whereas the Dufour effect is transmission of heat due to concentration gradients. This effect cannot be ignored in fluctuating systems with intense temperature gradients and high concentrations in progressions such as chemical production, material isolation, and many engineering activities. The human body needs to maintain its temperature to protect vital organs such as the heart, liver and brain. So, this phenomenon with radiation is usually observed in the maintenance of the temperature in the human body. Vasodilation of the skin and sweat removes excess heat energy generated by the organs through radiation and mixed convection. Thus, the current study exhibits all the aforementioned aspects in the presence of Arrhenius activation energy within Carreau nanofluids. The key results are discussed as follows.

4.1. Temperature Graphs

4.1.1. For the Thermal Radiation Parameter

The effects of R on the heat distribution profile are shown in Figure 2. For some fixed values $M = 0.3$, $Sr = Dr = \lambda^* = N_b = N_t = 0.1, \mathrm{Pr} = 1.5$ and $(R = 0.5, 0.7, 0.9, 1.1)$, variation is shown for θ. For the stretched flow, the influence of variation in the R parameter on temperature θ starts from the max value $\eta = 0$ until it approaches zero. Thus, the upshot in thermal emissivity adds more heat to the liquid, which causes a rise in temperature. The radiation parameter R has an increasing relationship with θ because R results in a striking increase in the internal kinetic energy of nanofluids, which is responsible for the temperature upshot, while the boundary layer thickness declines. It has been observed that a higher rate of thermal radiation postulates a larger heat flux.

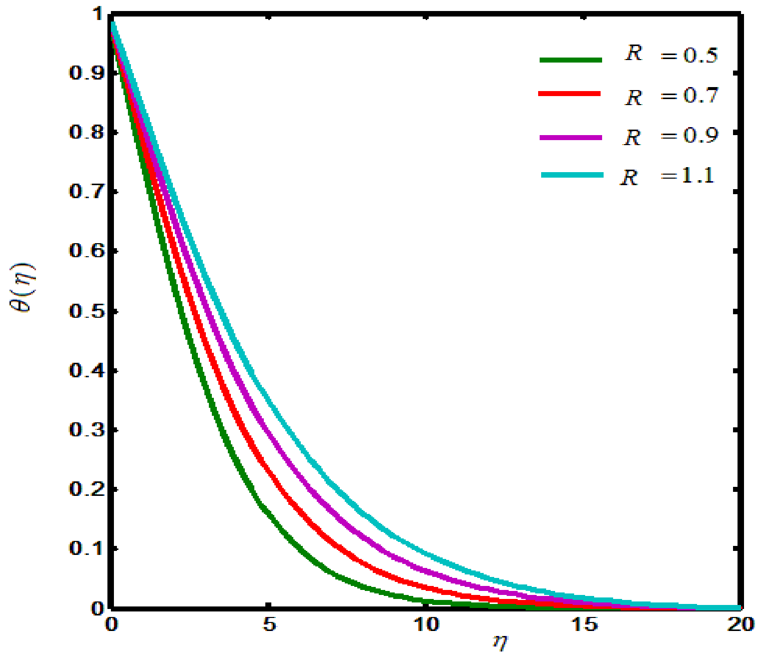

Figure 2. Impacts of R on $\theta(\eta)$.

4.1.2. For the Dufour Number

Figure 3 illustrates the role of the Dufour number (Dr) in temperature dispersion. It is evident that when ($Dr = 1.3, 1.5, 1.7, 1.9$) increases, then taking $M = 0.3$, $Sr = R = \lambda^* = N_b = N_t = 0.1, \Pr = 1.5$, the temperature of the fluid rises. In terms of thermal equations, the Dufour number is a result of the concentration gradient. The heating range is expanded due to the concentration gradient. This fact is supported by the mathematical formula $Dr = \frac{D_B K_T (C_f - C_\infty)}{\upsilon c_p c_s (T_f - T_\infty)}$. As a result, the fluid's viscosity decreases, its particles gain velocity, and an increase in its average temperature occurs.

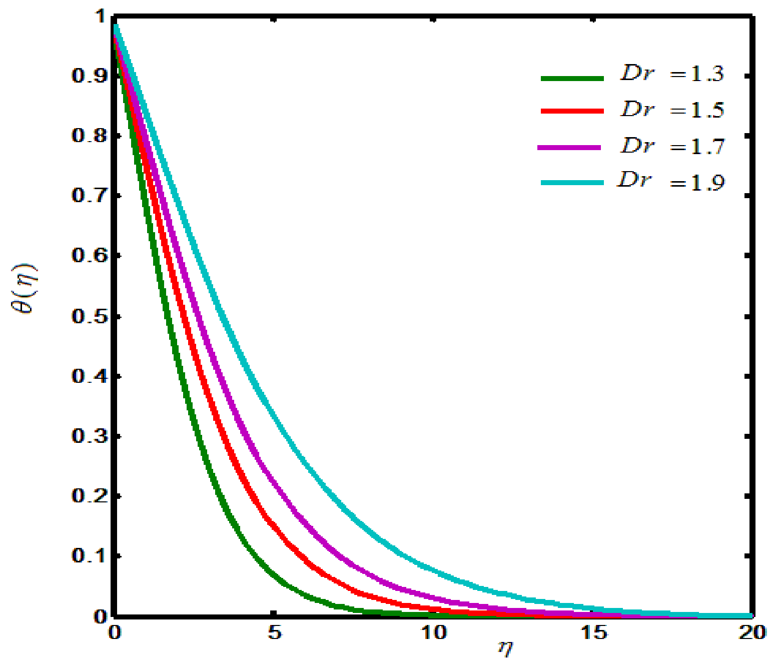

Figure 3. Impacts of Dr on $\theta(\eta)$.

4.1.3. For the Brownian Motion Parameter

Figure 4 depicts the curves for shear thinning ($n = 0.5$) fluid against θ when ($N_b = 0.3, 0.5, 0.7, 0.9$) and $M = 0.3$, $Sr = R = \lambda^* = Dr = N_t = 0.1, \Pr = 1.5$. The temperature trend enhances for upshot in N_b. Physically, more heat dispersion in the system is supported by the migration of thermophoretic nanoparticles. Nanoparticles move randomly and incoherently in Brownian motion. The temperature distribution rises as a result of the nanoparticles' high kinetic energy as the Brownian motion parameter is increased. The nanoparticle constitutes a major portion of the fortification of the heat transfer attributes of the Carreau liquid. The rising values of N_b increase the temperature and thermal thickness of the boundary layer. The Brownian motion force is influenced by the temperature gradient. The heating liquid particles are transported from a hotter surface to a colder exterior, increasing the thermal field. Therefore, a large number of nanoparticles are transported away from the surface intensely, which increases the temperature.

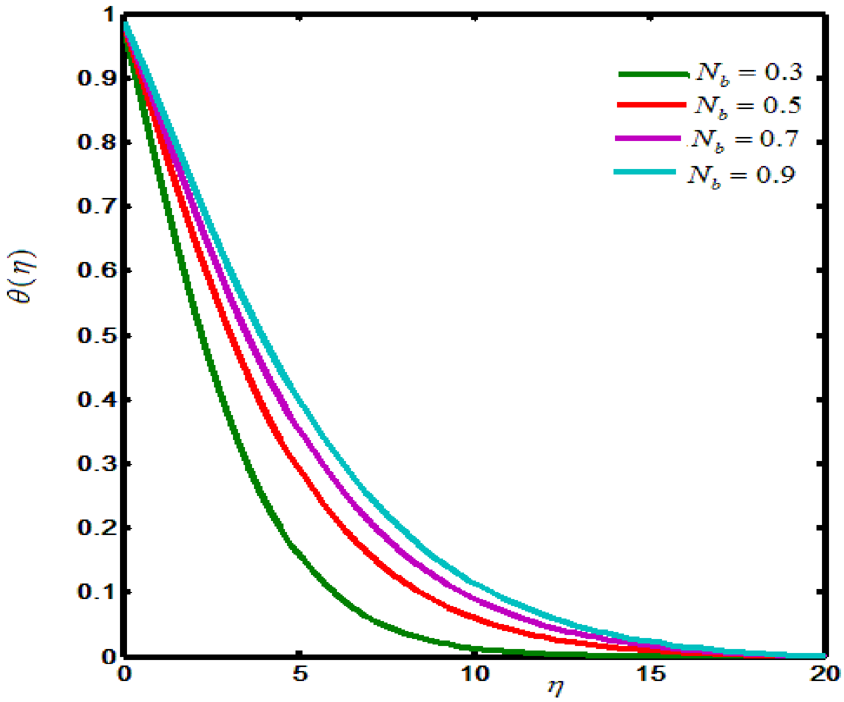

Figure 4. Impacts of N_b on $\theta(\eta)$.

4.1.4. For the Thermophoresis Parameter

Figure 5 shows the impact of N_t on the temperature profile. The inclined trend is noticed for n = 0.5, (shear thinning), with an increasing thermophoretic ($N_t = 0.3, 0.5, 0.7, 0.9$) nanoparticles inside the temperature field. Taking $M = 0.3$, $Sr = R = \lambda^* = Dr = N_b = 0.1, \Pr = 1.5$, a bulk of nanoparticles intensely transmit away from the surface, and hence increases the temperature of the Carreau liquid. Actually, a rise in the internal kinetic energy of nanoparticles causes thermophoresis diffusion. The increase in internal kinetic energy causes a faster heat transfer rate through the stretching sheet, which ultimately raises the temperature profile.

4.2. Concentration Graphs

4.2.1. For the Activation Energy Parameter

Figure 6 describes the effect of the parameter of activation energy E on the liquid's concentration ϕ. In this picture, the concentration profile $\phi(\eta)$ shows an increasing behavior when $E = 1.1, 1.3, 1.5, 1.7$, that is, the amount of energy required to start a chemical reaction is larger. We deduced that high activation energy E slows down chemical reaction mechanisms by reducing reaction rate. As a result, the nanofluid concentration rises.

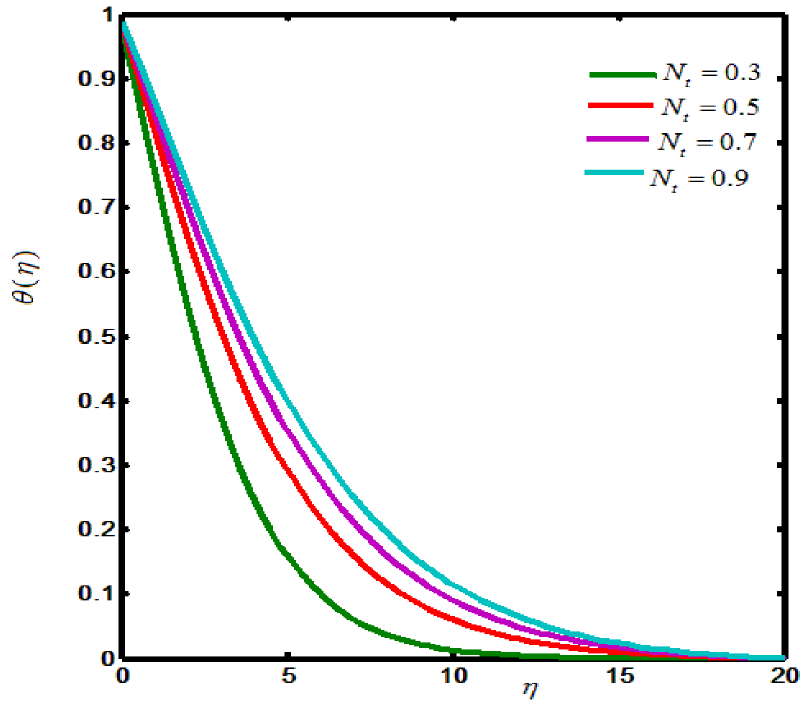

Figure 5. Impacts of N_t on $\theta(\eta)$.

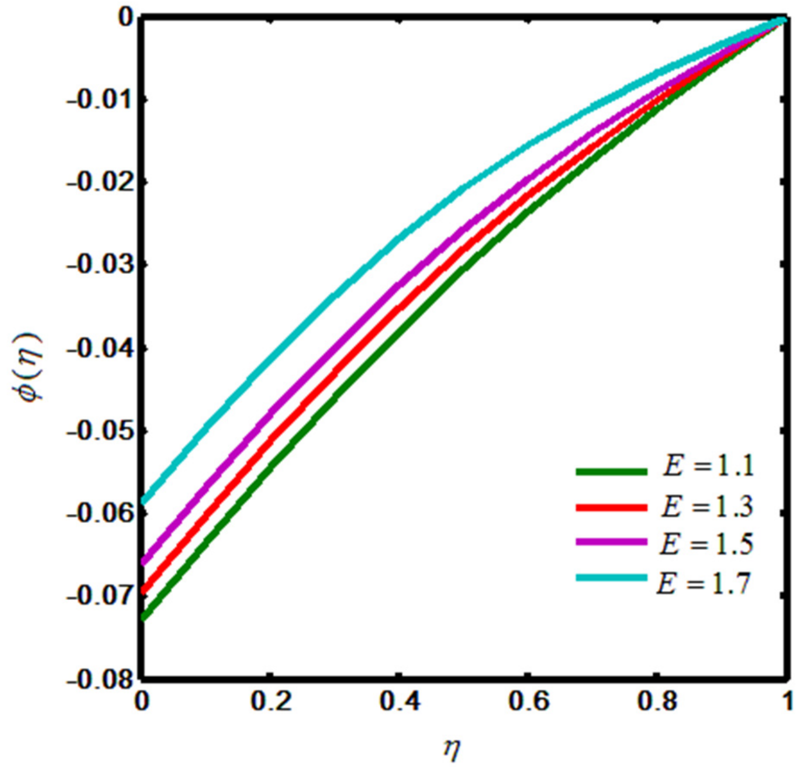

Figure 6. Impacts of E on $\phi(\eta)$.

4.2.2. For the Parameter of Brownian Motion

Figure 7 displays the nanofluid concentration profile for various ($N_b = 0.3, 0.5, 0.7, 0.9$) values. This graph demonstrates that when $M = 0.3$, $Sr = R = \lambda^* = Dr = N_b = 0.1$, $\Pr = 1.5$ and the N_b level rises, the concentration of the nanofluid drops. In physics, a random, incoherent motion of nanoparticles is termed Brownian motion. Thus, by raising the numeric value for N_b, the kinetic energy of the nanofluid rises, which reduces the fluid concentration.

Moreover, it is found that the rate at which nanoparticles fluctuate at various velocities physically increases with an uplift of N_b. Thus, the concentration trend is reduced because of the mobility of nanoparticles.

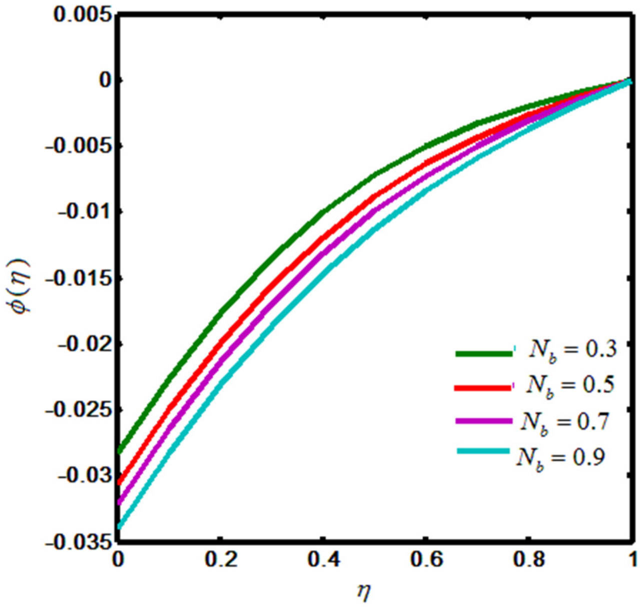

Figure 7. Impacts of N_b on $\phi(\eta)$.

4.2.3. For the Thermophoresis Parameter

Figure 8 is plotted to verify the effect of thermophoretic parameters on concentration distribution. This graph shows that the concentration of nanofluid decreases as N_t increases, that is, $(N_t = 0.3, 0.5, 0.7, 0.9)$. As diffusion penetrates deeper into the liquid, an upthrust in the thermophoretic causes thickening of the thermo-solutal layers at the boundary. Furthermore, it was discovered that an increase in the magnitude of N_t causes a physical rise with fluctuating speeds. As a result, the mobility of nanoparticles reduces the concentration profile.

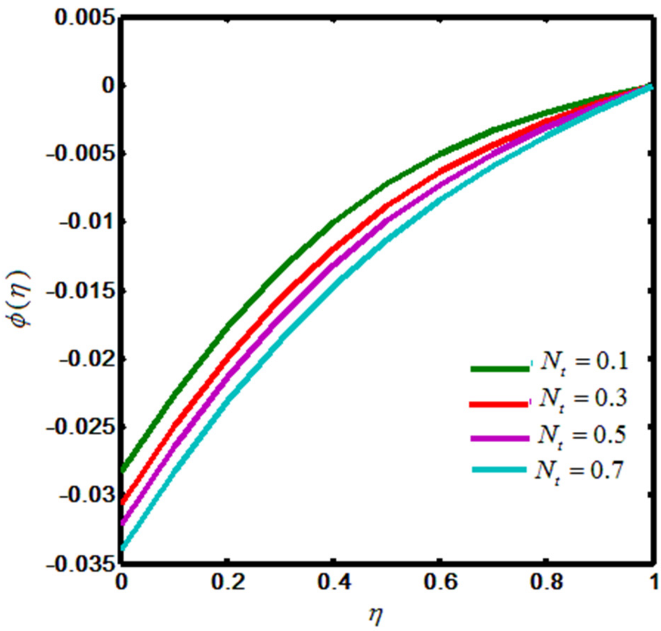

Figure 8. Impacts of N_t on $\phi(\eta)$.

4.2.4. For the Soret Number

Figure 9 shows the impact of the Soret number Sr on concentration. Increasing the Soret number ($Sr = 1.1, 1.3, 1.5, 1.7$) and the fixed parameters $M = 0.3$, $R = \lambda^* = Dr = N_t = N_b = 0.1, \Pr = 1.5$, the concentration distribution is effected and caused an increase in boundary layer viscosity. The Soret number Sr is generated from the thermal gradient in the concentration equation. The concentration gradient between the wall and the ambient fluid reduces as (Sr) increases, which is why particles gather and concentrate. The formula $Sr = \frac{D_B K_T (T_f - T_\infty)}{v T_m (C_f - C_\infty)}$ is used for the relative existence to describe this logical argument.

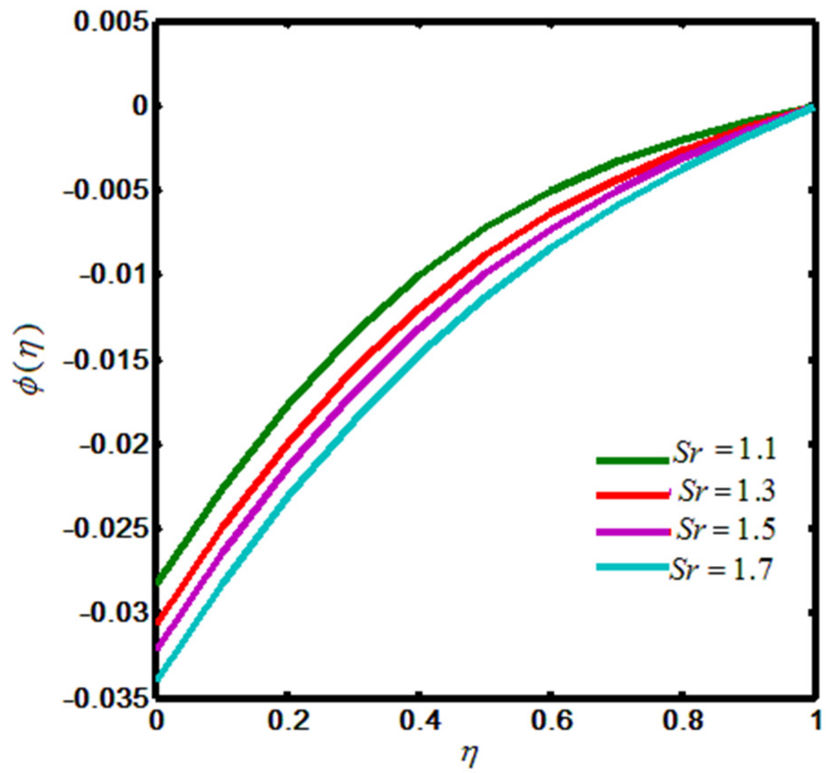

Figure 9. Impacts of Sr on $\phi(\eta)$.

4.2.5. For the Chemical Reaction Parameter and Fitted Rate Constant

Figure 10 shows the influence of the parameters of the chemical reaction on fluid concentration $\phi(\eta)$. The response of the concentration profile $\phi(\eta)$ is witnessed as a growing trend against rising chemical reaction parameter ($\Lambda = 1.1, 1.3, 1.5, 1.7$) values. As the chemical reaction parameter noticeably increases, the concentration of nanoparticles also rises. This upward tendency slows down by enhancing thermophoresis diffusion. Figure 11 shows that fluid concentration declines for higher values of fitted rate constant m.

4.3. Table Discussion

Tables 1 and 2 show values for $-f''(0)$ and $-g''(0)$ corresponding to a variety of values of α, i.e., $\alpha = 0, 0.25, 0.5, 0.75, 1$, whereas $N^* = We_1 = We_2 = 0$, $n = 1$. We conclude that the values for $-f''(0)$ and $-g''(0)$ show the assurance and accuracy of the applied method. The tabular form is utilized to represent the numerical survey. The effect of Pr on the transfer rate of heat is presented in Table 3. It was found that the higher numerical values for the rate of heat transfer $\widetilde{N}\widetilde{u}_x$ against various values of Prandtl number Pr that is Pr = 0.7, 2.0, 7.0, recorded assuming $N^* = We_1 = We_2 = \alpha = n = \lambda^* = N_b = N_t = Sr = Dr = \Lambda^* = Le = 0$ and found good agreement.

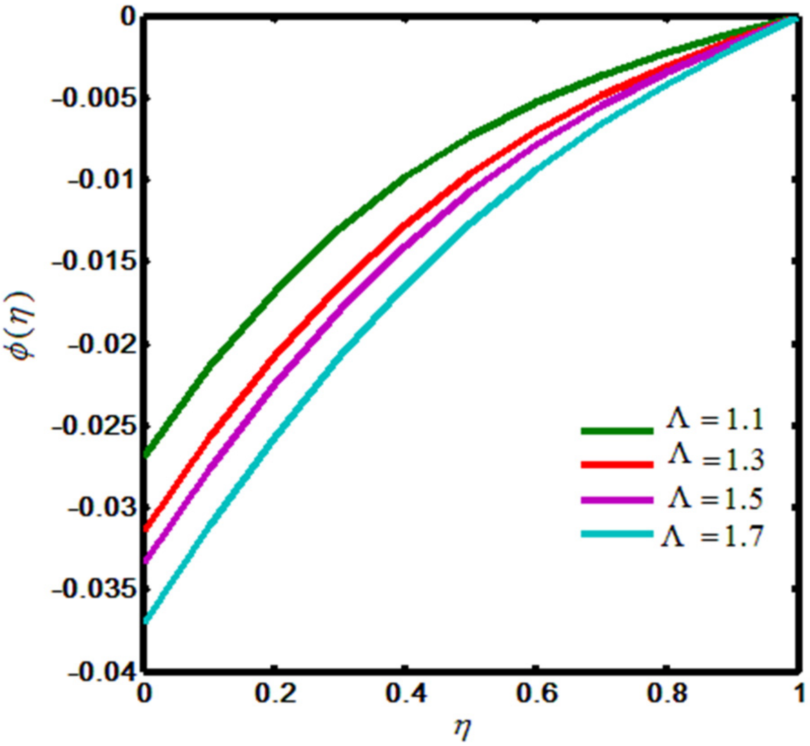

Figure 10. Impacts of Λ on $\phi(\eta)$.

5. Concluding Remarks

This study examines the effects of various variables on the temperature and concentration of the magnetohydrodynamic Carreau model with mixed convection, and the flow field is produced near the stretched sheet. The energy equation is equipped with nanofluid terms, thermal radiation and Dufour effects, while the Soret effect with activation energy is presented in the concentration equation subject to new mass flux condition. The Runge–Kutta–Fehlberg method with the shooting technique is used to sort the mathematical model. The R-K method is then used to solve the IVP with the proper initial approximations. The computed solution converges if boundary residuals $|y_i(\infty) - \widetilde{y}_i(\infty)|$ for $(i = 2, 5, 7, 9)$, where $\widetilde{y}_i(\infty)$ are computed values, are smaller than tolerance errors, or 10^{-6} (see Figure 11). The operation is repeated until the outcome complies with the predicted convergence principle if the computed results did not meet these criteria (see Figure 12). Due to the variable nature of the involved physical parameters, their aftermath is displayed in tables and graphs. The drag forces $f''(0)$ and $g''(0)$ against stretching ratio parameter $\alpha = 0, 0.25, 0.50, 0.75$ are shown in Tables 1 and 2. The numerical values for the rate of heat transfer $\widetilde{N}\widetilde{u}_x$ are shown in Table 3. For various of values of Prandtl number Pr that is Pr = 0.7, 2.0, 7.0, increasing values of $Nu_x = 0.454525$, 0.91213, 1.876201, respectively, are recorded for $N^* = We_1 = We_2 = \alpha = n = \lambda^* = N_b = N_t = Sr = Dr = \Lambda^* = Le = 0$, which are in good agreement with Ref. [13]. The estimated errors are defined as error $= \frac{|Nu_x| - |\widetilde{N}\widetilde{u}_x|}{|\widetilde{N}\widetilde{u}_x|}$, which gives 0.0052%, 0.079% and 1.9199%. These errors show that the current study has accurate readings, as by eliminating some specific terms, this problem can be reduced to Ref. [13]. This shows the correct novelty of the proposed problem. Further, the temperature of nanofluid θ will rise as the radiation parameter $(R = 0.5, 0.7, 0.9, 1.1)$ and the Dufour number $(Dr = 1.3, 1.5, 1.7, 1.9)$ increase. The thermophoresis and Brownian motion parameters $(N_b,\ N_t)$ intensify the temperature profile, but the opposite behavior is shown for $(N_b,\ N_t)$ upon fluid concentration. The activation energy E and fitted rate constant m heighten the curves of fluid concentration, whereas the reverse trend is observed for the Soret number Sr and chemical reaction parameter Λ.

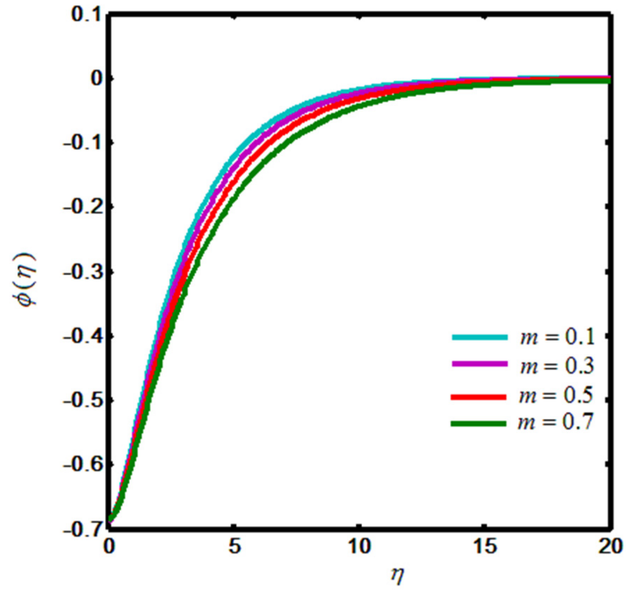

Figure 11. Impacts of m on $\phi(\eta)$.

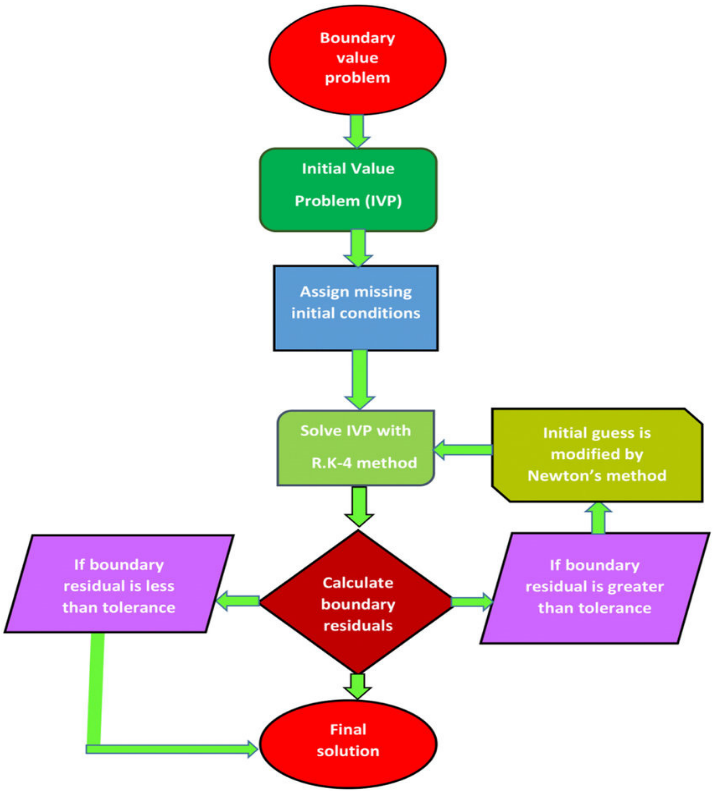

Figure 12. Flow chart for the shooting method.

Author Contributions: Conceptualization, U.A.; methodology, U.A.; validation, U.A.; writing—original draft, U.A.; writing—review and editing, U.A.; formal analysis, M.O. and U.A.; investigation, M.O.; funding acquisition, U.A. All authors have read and agreed to the published version of the manuscript.

Funding: This research was supported by the Zhejiang Normal University Research Fund under Grant YS304222980.

Data Availability Statement: No data were used for the research in this article. It is pure mathematics.

Conflicts of Interest: The authors declare that they have no conflict of interest.

Nomenclature

(u, v, w)	Velocity components (m/s)
U_w, V_w	Stretching velocity
	Free stream velocity
a, b	Stretching constant
T, T_∞	Surface temperature, ambient temperature (K)
C, C_∞	Surface concentration, ambient Concentration
c_p	Specific heat at constant pressure $(\mathrm{J}/\mathrm{kgK})$
D_M	Mass diffusivity
We_1, We_2	Local Weissenberg number
p	Pressure $\left(\mathrm{N}/\mathrm{m}^2\right)$
n	Power law index
I	Identity tensor
A_1	First Rivlin Erickson tensor
Pr	Prandtl number
Sc	Schmidt number
k	Thermal conductivity (W/mK)
Re_x	Local Reynolds number
k_c	Reaction rate constant
D_B, D_T	Brownian motion and thermophoresis diffusion coefficients $\left(\mathrm{m}^2/\mathrm{s}\right)$
$B_\circ$	Magnetic field coefficient
M	Magnetic field parameter
q_r	Roseland radiative heat flux, $\left(\mathrm{W}/\mathrm{s}^2\right)$
k^*	Absorption coefficient $(1/\mathrm{m})$
R	Thermal radiation parameter
N_t, N_b	Thermophoresis parameter, Brownian motion parameter
Le	Lewis number
N^*	Buoyancy ratio parameter
Pr	Prandtl number
Dr, Sr	Dufour and Soret numbers
g	Gravitational acceleration $\left(\mathrm{m}/\mathrm{s}^2\right)$
E^*	Activation energy
m	Fitted rate constant
Greek letters	
η	Similarity variable
θ	Dimensionless temperature
ϕ	Dimensionless concentration
μ	Apparent viscosity $(\mathrm{kg}/\mathrm{ms})$
ρ_f	Density of fluid $\left(\mathrm{kg}/\mathrm{m}^3\right)$
τ_w	Surface shear stress
$\hat{\tau}$	Cauchy stress tensor
$\mu_\circ$, μ_∞	Zero shear rate viscosity, infinite shear rate viscosity $(\mathrm{kg}/\mathrm{ms})$
λ^*	Mixed convection parameter
ψ	Stream function
β_T, β_C	Thermal and concentration expansion coefficient
v	Kinematic viscosity $\left(\mathrm{m}^2/\mathrm{s}\right)$
α_1	Thermal Diffusivity $\left(\mathrm{m}^2/\mathrm{s}\right)$
α	Velocity ratio parameter
Λ	Chemical reaction parameter
Δ^*	Temperature difference parameter
$\overset{\bullet}{\gamma}$	Second invariant strain tensor
σ	Electrical conductivity
σ^*	Stefan–Boltzman constant
Γ	Material time constant
κ	Boltzmann constant

References

1. Choi, S.U.; Eastman, J.A. *Enhancing Thermal Conductivity of Fluids with Nanoparticles (No. ANL/MSD/CP-84938; CONF-951135-29)*; Argonne National Lab. (ANL): Argonne, IL, USA, 1995.
2. Buongiorno, J. Convective Transport in Nanofluids. *J. Heat Transfer.* **2006**, *128*, 240–250. [CrossRef]
3. Xuan, Y.; Li, Q. Heat transfer enhancement of nanofluids. *Int. J. Heat Fluid Flow* **2000**, *21*, 58–64. [CrossRef]
4. Rashidi, M.; Ganesh, N.V.; Hakeem, A.A.; Ganga, B. Buoyancy effect on MHD flow of nanofluid over a stretching sheet in the presence of thermal radiation. *J. Mol. Liq.* **2014**, *198*, 234–238. [CrossRef]
5. Malvandi, A.; Hedayati, F.; Ganji, D. Slip effects on unsteady stagnation point flow of a nanofluid over a stretching sheet. *Powder Technol.* **2014**, *253*, 377–384. [CrossRef]
6. Das, P.K. A review based on the effect and mechanism of thermal conductivity of normal nanofluids and hybrid nanofluids. *J. Mol. Liq.* **2017**, *240*, 420–446. [CrossRef]
7. Atashafrooz, M.; Sajjadi, H.; Delouei, A.A. Simulation of combined convective-radiative heat transfer of hybrid nanofluid flow inside an open trapezoidal enclosure considering the magnetic force impacts. *J. Magn. Magn. Mater.* **2023**, *567*, 170354. [CrossRef]
8. Wang, G.; Zhang, J. Thermal and power performance analysis for heat transfer applications of nanofluids in flows around cylinder. *Appl. Therm. Eng.* **2017**, *112*, 61–72. [CrossRef]
9. Ali, U.; Malik, M.; Alderremy, A.; Aly, S.; Rehman, K.U. A generalized findings on thermal radiation and heat generation/absorption in nanofluid flow regime. *Phys. A Stat. Mech. Its Appl.* **2020**, *553*, 124026. [CrossRef]
10. Carreau, P.J. Rheological Equations from Molecular Network Theories. *Trans. Soc. Rheol.* **1972**, *16*, 99–127. [CrossRef]
11. Carreau, P.J.; De Kee, D.; Daroux, M. An analysis of the viscous behaviour of polymeric solutions. *Can. J. Chem. Eng.* **1979**, *57*, 135–140. [CrossRef]
12. Eid, M.R.; Mahny, K.L.; Muhammad, T.; Sheikholeslami, M. Numerical treatment for Carreau nanofluid flow over a porous nonlinear stretching surface. *Results Phys.* **2018**, *8*, 1185–1193. [CrossRef]
13. Khan, M.; Sardar, H.; Gulzar, M.M.; Alshomrani, A.S. On multiple solutions of non-Newtonian Carreau fluid flow over an inclined shrinking sheet. *Results Phys.* **2018**, *8*, 926–932. [CrossRef]
14. Akbar, N.; Nadeem, S.; Haq, R.U.; Ye, S. MHD stagnation point flow of Carreau fluid toward a permeable shrinking sheet: Dual solutions. *Ain Shams Eng. J.* **2014**, *5*, 1233–1239. [CrossRef]
15. Machireddy, G.R.; Naramgari, S. Heat and mass transfer in radiative MHD Carreau fluid with cross diffusion. *Ain Shams Eng. J.* **2018**, *9*, 1189–1204. [CrossRef]
16. Raza, R.; Mabood, F.; Naz, R. Entropy analysis of non-linear radiative flow of Carreau liquid over curved stretching sheet. *Int. Commun. Heat Mass Transf.* **2020**, *119*, 104975. [CrossRef]
17. Salahuddin, T.; Awais, M.; Xia, W.-F. Variable thermo-physical characteristics of Carreau fluid flow by means of stretchable paraboloid surface with activation energy and heat generation. *Case Stud. Therm. Eng.* **2021**, *25*, 100971. [CrossRef]
18. Huang, C.-J. Influence of non-Darcy and MHD on free convection of non-Newtonian fluids over a vertical permeable plate in a porous medium with soret/dufour effects and thermal radiation. *Int. J. Therm. Sci.* **2018**, *130*, 256–263. [CrossRef]
19. Mahabaleshwar, U.; Nagaraju, K.; Kumar, P.V.; Nadagouda, M.; Bennacer, R.; Sheremet, M. Effects of Dufour and Soret mechanisms on MHD mixed convective-radiative non-Newtonian liquid flow and heat transfer over a porous sheet. *Therm. Sci. Eng. Prog.* **2020**, *16*, 100459. [CrossRef]
20. Seid, E.; Haile, E.; Walelign, T. Multiple slip, Soret and Dufour effects in fluid flow near a vertical stretching sheet in the presence of magnetic nanoparticles. *Int. J. Thermofluids* **2022**, *13*, 100136. [CrossRef]
21. Falodun, B.O.; Ayegbusi, F.D. Soret–Dufour mechanism on an electrically conducting nanofluid flow past a semi-infinite porous plate with buoyancy force and chemical reaction influence. *Numer. Methods Partial. Differ. Equ.* **2021**, *37*, 1419–1438. [CrossRef]
22. Reddy, N.N.; Reddy, Y.D.; Rao, V.S.; Goud, B.S.; Nisar, K.S. Multiple slip effects on steady MHD flow past a non-isothermal stretching surface in presence of Soret, Dufour with suction/injection. *Int. Commun. Heat Mass Transf.* **2022**, *134*, 106024. [CrossRef]
23. Hayat, U.; Shaiq, S.; Shahzad, A.; Khan, R.; Kamran, M.; Shah, N.A. The Effect of Particle Shape on Flow and Heat Transfer of Ag-Nanofluid along Stretching Surface. *Chin. J. Phys.* **2023**. [CrossRef]
24. Wang, C.Y. The three-dimensional flow due to a stretching flat surface. *Phys. Fluids* **1984**, *27*, 1915. [CrossRef]
25. Ali, U.; Malik, M.; Rehman, K.U.; Alqarni, M. Exploration of cubic autocatalysis and thermal relaxation in a non-Newtonian flow field with MHD effects. *Phys. A Stat. Mech. Its Appl.* **2020**, *549*, 124349. [CrossRef]